

Role of dual SiO_x:H based buffer at the p/i interface on the performance of single junction microcrystalline solar cells



Gourab Das^{a,*}, Sourav Mandal^a, Sukanta Dhar^a, Sukanta Bose^a, Sumita Mukhopadhyay^a, Chandan Banerjee^b, Asok K. Barua^a

^a Centre of Excellence for Green Energy and Sensor Systems, Indian Institute of Engineering Science & Technology, Shibpur, Howrah-711103, India

^b National Institute of Solar Energy, Gwalpahari, Gurgaon 122003, Haryana, India

ARTICLE INFO

Keywords:

Oxide based microcrystalline silicon
Dual buffer
PECVD
Material properties
Solar cells

ABSTRACT

In p-i-n structure a-Si solar cell a buffer layer with proper characteristics plays important role in improving the p/i interface of the cell, reducing mismatch of band gaps and number of recombination centres. However for p-i-n structure microcrystalline (μ -Si:H) cell which has much less light induced degradation than a-Si:H cell, not much work has been done on development of proper buffer layer and its application to μ -Si:H cell. In this paper we have reported the development of two intrinsic oxide based microcrystalline layer having different characteristics for use as buffer layers at the p/i interface of μ -Si:H cell. Previously SiO_x:H buffer layer has been used at the p/i interface which showed positive effects. To explore the possibility of improving the performance of p-i-n structure μ -Si:H cell further we have thought it interesting to use two buffer layers with different characteristics at the p/i interface. The two buffer layers have been characterized in detail and applied at the p/i interface of the μ -Si:H cell with positive effects on all the PV parameters mainly improves the open circuit voltage (V_{oc}) and enhances short circuit current (I_{sc}). The maximum initial efficiency obtained is 8.97% with dual buffer which is 6.7% higher than that obtained by using conventional single buffer layer at the p/i interface. Stabilized efficiency of the cell with dual buffer is found to be \sim 9.5% higher than that with single buffer after 600 h of light soakings.

1. Introduction

Amongst silicon based thin film solar cells micromorph has good potential of competing with c-Si cells when the production volume is in the terawatt range and the stabilized module efficiency of micromorph is 15% and above. In a micromorph cell the microcrystalline (μ -Si:H) cell is the bottom and a-Si cell is the top cell. The bottom cell shows very little light induced integration [1–4] which is its basic advantage. To improve the performance of μ -Si:H cell is therefore now a priority area in photovoltaic (PV) cell research and development activities.

One of the major downside of the single junction μ -Si:H solar cell is its low open circuit voltage as compared to a-Si silicon solar cell [5,6]. Although there is a large impact of crystalline volume fraction on V_{oc} of the μ -Si:H solar cell, carrier recombination at the p-i interface region plays a considerable role to minimize V_{oc} of the cell. Comprehensive research is going on to overcome the drawbacks. Various approaches have been taken to improve the V_{oc} . Use of a thin μ -Si:H buffer layer deposited by hot-wire chemical vapour deposition (HW-CVD) system was shown to significantly improve the V_{oc} in single junction μ -Si:H

solar cells [7,8]. Wide band gap window layer is one of common method to enhance the performance of single junction a-Si:H as well as μ -Si:H solar cell [9–12]. In recent times many other research activities is going on improve the performance of single junction μ -Si:H solar cell by various method [13–18].

In an earlier paper we have shown [19] the improvement in the performance of p-i-n structure a-Si solar cell by using intrinsic oxide based buffer layer at the p/i interface. For μ -Si:H Bugnon et al. have successfully used SiO_x:H buffer layer at the p/i interface of microcrystalline cell with positive results [20].

To obtain the beneficial effect of using buffer layer with proper characteristics we thought it worthwhile to employ double buffer layer with different characteristics to further improve the performance of microcrystalline cell. By using two buffer layers with proper characteristics we have been able to improve short circuit current and open circuit voltage of microcrystalline cell significantly. This new approach has given interesting results which can be explored further.

* Corresponding author.

E-mail address: gourab_electron@hotmail.com (G. Das).

2. Experimental details

Oxide based materials and single junction microcrystalline silicon solar cells are fabricated using capacitively coupled five chamber cluster RF-PECVD systems. We used 13.56 MHz rf- frequency for doped and oxide based layers and 27.12 MHz for intrinsic absorber layer. Semiconductor grade SiH₄, H₂, CO₂, B₂H₆, PH₃ gases were used to develop different layer of the solar cell. SiH₄, H₂, B₂H₆ and CO₂ gas were used to make oxide based p-layer with optimized process parameters. Flow ratio of CO₂ to SiH₄ (CO₂/SiH₄) was optimized with 0.5 for developing microcrystalline window layer. SiH₄, H₂ and CO₂ gases were employed to develop buffer layers and CO₂/SiH₄ of 0.4 and 0.25 were adopted to make a buffer of two different characteristics. We used the same chamber for developing p-layer and buffer layers for fabrication of solar cell. After making of window layer i.e. p-layer chamber was flushed with the H₂ plasma for 15 min followed by a thin a-Si coating by SiH₄ and H₂ to decontaminate the chamber. Intrinsic absorber layer (i-μc-Si: H) was developed in separate chamber in high power pressure regime with the help of SiH₄ and H₂. 1% PH₃ in SiH₄ and H₂ gases were used to develop n-type films.

The films are deposited on Na/K free Schott glass and one side polished silicon wafer for various characterizations. Stylus type profilometer (Bruker Dektak-XT) was used to measure the thicknesses of the films. Dark conductivity (σ_d) was measured at room temperature in a cryostat evacuated at the range of $\sim 10^{-5}$ Torr, after making co-planar metal electrode of aluminum deposited by thermal evaporation. The conductivity was calculated using the formula:

$$\sigma_d = (w \times I) / (l \times d \times V) \quad (1)$$

where l = length of the electrode, d = film thickness, w = separation between two electrodes, I = Current and V = applied voltage. Activation energy (E_a) was calculated from the slope of $\ln \sigma_d$ vs $10^3/T$ plot [19]. Atomic Force Microscopy (NT-MDT) and High Resolution-Transmission Electron Microscopy studies ((HRTEM JEOL-JSM 20100) are employed to explore the structural properties of the films. The crystalline volume fraction (X_c) of the films was estimated using Raman spectroscopy (Lab RAM HR-Argon ion laser, wavelength-514 nm in back scattering geometry). X_c was calculated from the integrated intensities of Raman peak at 480 cm⁻¹, 510 cm⁻¹ and 520 cm⁻¹ using the formula,

$$X_c = (I_{510} + I_{520}) / (I_{480} + I_{510} + I_{520}) \quad (2)$$

The XRD analysis of the micro/nano crystalline materials was procured by a high resolution X-ray diffractometer (PANALYTICAL XPERT PRO). Perkin-Elmer Spectrum Two spectrometer in absorption mode was used to accomplished FTIR spectroscopy. Atomic percent of oxygen C(O) incorporated in the film was estimated from the integrated absorption strength of Si-O-Si stretching absorption band around 900–1200 cm⁻¹ following Lucovsky *et al.* [21]. Optical gap of microcrystalline material can be often expressed as the photon energy at which absorption coefficient (α) = 10^4 cm⁻¹ which is also known as E_{04} . The optical absorption (E_{04}) was evaluated from UV-visible spectroscopic data.

I - V characteristics of all the fabricated solar cell have been measured under standard test conditions i.e. at AM 1.5 G, 30 °C and 1000 W/m² and spectral response was measured in Bentham PVE300 setup.

3. Results and discussions

3.1. Material characterizations

Optimized process parameters for deposition of microcrystalline p-SiO_x:H, intrinsic absorber and n-type layer is shown in Table 1. High quality intrinsic layer [22] of microstructure factor (r) = 0.038, calculated after deconvolution of the FTIR spectrum at 2000 cm⁻¹ and around 2070–2090 cm⁻¹ respectively [23] using the formula,

$$r = I_{2070} / (I_{2000} + I_{2070}) \quad (3)$$

was used as active layer. FTIR spectrum of the intrinsic absorber layer is shown in Fig. 1.

Influence of CO₂/SiH₄ on the intrinsic buffer layer was investigated in details. Table 2 shows the process parameters for developing oxide based microcrystalline buffer layer with its optoelectronics and structural properties. As CO₂/SiH₄ = 0.5 was used to develop p-layer (described in Table 1), we evolved mso-1 layer with CO₂/SiH₄ = 0.4 and followed by 0.25 for mso-2 layer. From Fig. 2 it is clear that peak height around the 1000–1200 cm⁻¹ which is due to Si-O-Si bonding [21] increases gradually as we increase the CO₂/SiH₄ ratio for the deposited films. It can be seen that peak height is highest for p-layer followed by mso-1 and mso-2. It is also seen from Fig. 2 that with the decrease of CO₂/SiH₄, peak around the 2000 cm⁻¹ tends to increase which was good for solar cell application [24]. As a result of increasing peak height around 1000–1200 cm⁻¹, indicates the more amount of atomic oxygen (O) incorporated in the films microstructure, optical gap (E_{04}) of the p-μc-SiO:H layer is found to be highest which is 2.35 eV. E_{04} of mso-1 and mso-2 are 2.18 eV and 2.02 eV respectively which was shown in Fig. 3. From the absorption curve (Fig. 3) it is seen that optical gap of the intrinsic layer (i-μc-Si: H) is lowest among all which is 1.86 eV. From the Table 2, it is seen that dark conductivity (σ_d) of the films decreases from 1.1×10^{-4} S/cm (mso-1) to 3.0×10^{-5} S/cm (mso-2) as the CO₂/SiH₄ decreases from 0.4 to 0.25. This is due to defects introduced in the films if more atomic oxygen is incorporated which leads to greater disorder in the film resulting higher dark conductivity. But activation energy (E_a) increases to 0.49 eV from 0.41 eV as CO₂/SiH₄ decreases indicates the evolution of better quality microcrystalline films.

Raman spectroscopy analysis assists us to determine crystalline volume fraction (X_c) of the micro/nano crystalline films. X_c is calculated to be 51% for mso-1% and 62% for mso-2. As the O-content in mso-2 film is lower than the mso-1 film, X_c is higher for the film mso-1. It is clear indication that atomic oxygen hinders the growth of crystallinity [25]. That is why X_c increases as CO₂/SiH₄ decreases (Fig. 4). It could be also seen from the Fig. 4 that as CO₂/SiH₄ decreases peak point of the curve shifted towards the 520 cm⁻¹ which is the evidence of evolution of crystallites with larger grain size.

Fig. 5 shows the X-ray diffractogram of mso-1 and mso-2 films for a scattering angle between 25° and 60°. The XRD spectra shows three distinct peaks at $2\theta = 28.44^\circ$, 47.30° and 56.12° that correspond to the $\langle 111 \rangle$, $\langle 220 \rangle$ and $\langle 311 \rangle$ crystallographic planes of Si [26]. This indicates that the crystallites have grown on all possible direction. $\langle 111 \rangle$ and $\langle 220 \rangle$ peaks are more prominent than the $\langle 311 \rangle$ peaks. It is clear from the Fig. 5 that peak height around $\langle 111 \rangle$ and $\langle 220 \rangle$ are increases with decrease of CO₂/SiH₄ which is a clear indication of growth of more crystallites. The average size of the crystallites of these oxide based microcrystalline silicon films has been calculated using Debye-Scherrer formula [27]. As the CO₂/SiH₄ decreases from 0.4 to 0.25, average particle size increases to 14.4 nm from 11.7 nm which is probably due to more atomic oxygen in the films hamper the growth of crystallites in the films.

Microstructure, surface morphology and surface roughness of the intrinsic oxide based microcrystalline films have been investigated by AFM. Fig. 6 shows the AFM surface morphology of the i-μc-SiO:H films (mso-1 and mso-2). It is clear from the Fig. 6 that there is larger grain size noticed in mso-2 film as compare to mso-1 film. Average grain size is also estimated from the AFM micrograph and the results are agreed well with the grain size obtained from XRD analysis. RMS roughness of mso-2 films is also higher which is 77.36 nm rather than 39.61 nm for mso-1 layer. The more crystalline films have more roughness as a result light absorption will be more.

We have also compared the Raman spectra of the i-layers deposited without any seed layer, mso-1 and mso-2 as seed layer (Fig. 7). It is observed that high X_c of 66% of the i-layer grown on 5 nm of mso-2

Table 1
Optimized deposition condition of individual layer for single junction μ -Si:H solar cell solar cell.

Materials	$\text{SiH}_4 / \text{H}_2$	B_2H_6 (sccm)	PH_3 (sccm)	CO_2/SiH_4 (sccm)	P_d (mW/cm ²)	P_r (torr)	X_c (%)	σ_d (S/cm)	E_a (eV)
p- μ -SiO:H	1:100	0.8	NA	0.5	50	0.5	42	0.91	0.041
i- μ -Si:H	1:33.33	NA	NA	NA	300	5	57	5.8E-6	0.55
n- μ -Si:H	1:45	NA	0.04	NA	40	1	67	67	0.019

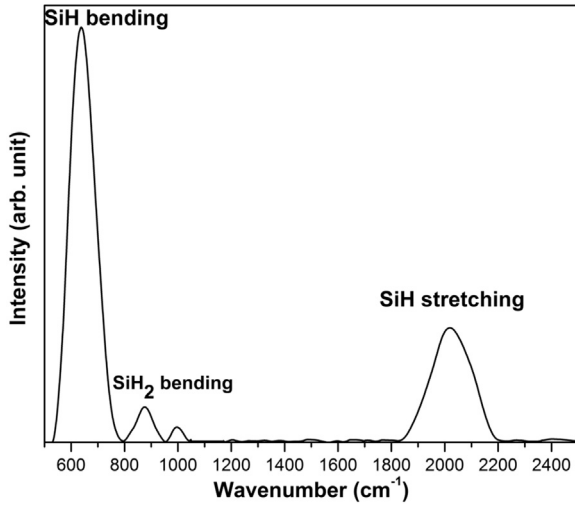


Fig. 1. FTIR spectrum of the optimized intrinsic μ -Si:H material.

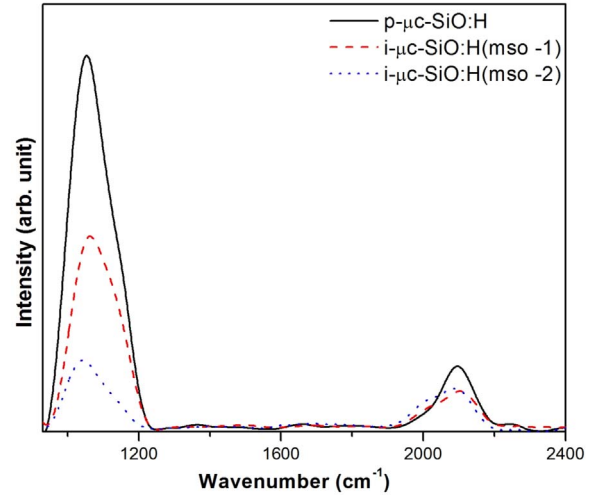


Fig. 2. FTIR spectra of oxides based window and buffer layers.

layer. X_c is 57% when no seed layer has been used to evolve i-layer (Fig. 7).

3.2. Application of i- μ -SiO:H films as dual buffer in single junction microcrystalline silicon solar cells

The aim of this investigation is to develop suitable i-type μ -SiO:H films with proper characteristics and the effects of applying these materials as dual buffer in the fabrication of single junction μ -Si:H solar cells. Textured ZnO:Al is used as transparent conducting oxide (TCO) of the fabricated cells. Single junction a-Si solar cells of area 1 cm² have been fabricated with the following structures (shown in Fig. 8) and utilizing the material described in Tables 1, 2,

Glass/ZnO:Al/p- μ -SiO:H/i- μ -SiO:H (mso-1)/i- μ -Si:H/n- μ -Si:H/Al (cell-49).

Glass//ZnO:Al/p- μ -SiO:H/i- μ -SiO:H (mso-1) + i- μ -SiO:H (mso-2)/i- μ -Si:H/n- μ -Si:H/Al (cell-55).

The solar cell with single buffer layer (with mso-1) has been fabricated (shown in Fig. 8 and the PV parameters are as follows:

Short circuit current (I_{sc}) = 25.77 mA, open circuit voltage (V_{oc}) = 0.502 V, fill factor (FF) = 65% and efficiency (η) = 8.41%. I - V curve is shown in Fig. 10 (cell 49).

We have used mso-1 and mso-2 films for solar cell fabrication (properties shown in Table 2). Single junction μ -Si:H solar cell performances were evaluated by using these layers as dual buffer at the p/i interface.

Table 2
Deposition condition and characteristics of mso-1 and mso-2 layers.

Sample No.	$\text{SiH}_4 / \text{H}_2$	$\text{CO}_2 / \text{SiH}_4$	P_w (mW/cm ²)	Dep rate ($\text{\AA}/\text{min}$)	σ_d (S cm ⁻¹)	E_a (eV)	E_{04} (eV)	X_c (%)	Particle size from XRD (nm)
mso-1	1:100	0.4	50	6.0	1.1E-4	0.41	2.18	51	11.7
mso-2		0.25		6.2	3.0E-5	0.49	2.02	62	14.4

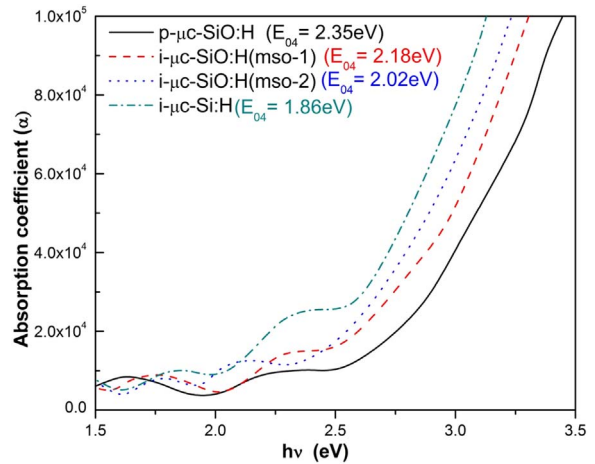


Fig. 3. Absorption co-efficient vs. $h\nu$ spectra of the oxide based films and intrinsic films.

We have separately optimized the thickness of the individual buffer layer for the fabrication of solar cell and found the suitable thickness for first buffer is 3.0 nm and second one of 4.0 nm. The optimized thickness of the each and every individual layer of fabricated solar cells was also shown in Fig. 8. Schematic band diagram of the single junction μ -Si:H solar cell with dual buffer is shown in Fig. 9.

By using this optimized dual buffer in place of conventional single buffer layer at the p/i interface (Fig. 8, cell 55) I_{sc} , V_{oc} , FF is increased by 1.4%, 3.5%, 1.5% respectively and η is increased by 6.7%. I_{sc} is

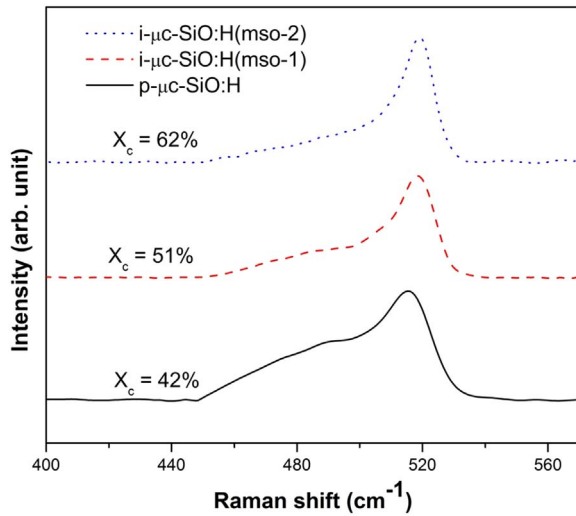


Fig. 4. Comparison of Raman spectra of oxide based microcrystalline films.

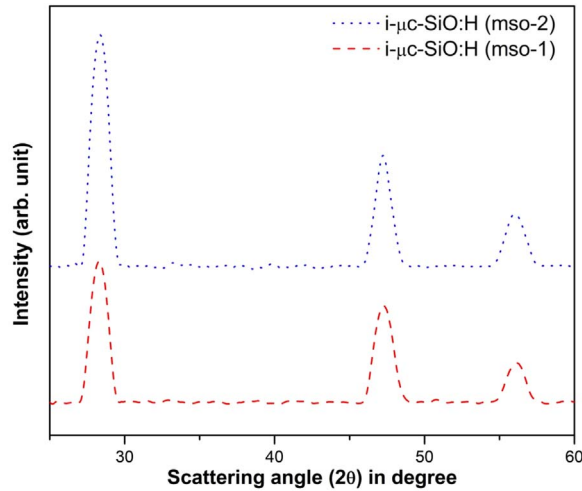


Fig. 5. XRD spectra of mso-1 and mso-2 films.

increased may be due the better nucleation of the i-layer as the X_c of the mso-2 is around 62% with larger grain size (14.4 nm), which is act as a growth zone or seed layer of the intrinsic hydrogenated microcrystalline silicon films. V_{oc} and FF are improved due to better elimination of band gap mismatching problem between high band gap window layer

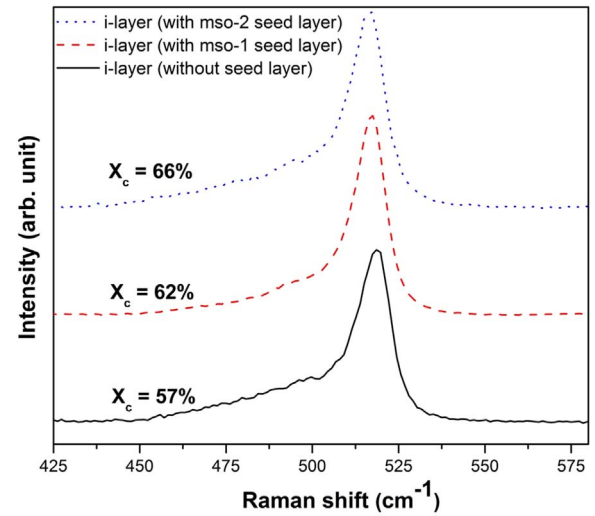


Fig. 7. Comparison of Raman spectra of the i-layer without any seed layer, mso-1 as seed layer and mso-2 as seed layer.

($E_{04} = 2.35$ eV) and absorber layer ($E_{04} = 1.86$ eV) leads to serious reduction of p/i interface recombination or trap center. 2nd buffer layer (mso-2) may have also a role of protecting layer of 1st buffer layer (mso-1) as intrinsic absorber layer was deposited in very high power which leads to poor interface between p-layer and active layer. Dual buffer layer may also help to reduce the unintentional boron-doping at the absorber layer further which results the better solar cell output [20] (Fig. 10).

We are demonstrating the increment in the I_{sc} using dual buffer at the p/i interface by using EQE measurements (Fig. 11). It can be seen clearly that there is an improvement in the collection over the blue region of the solar spectrum. Enhanced collection in the blue region is the clear indication of reduction in boron cross-contamination from the p-layer to the i-layer and also linked to an improvement of the i-layer nucleation as highly crystalline mso-2 layer here acts as seed layer [20]. Buffer layer of less O-content (mso-2) may also contribute to the total current of the cell. That could be also reasons for enhancement in the spectral response in the blue part of sun's spectrum.

We have also investigated the solar cell performances after 600 h of light soakings. It is well noticed that microcrystalline cell with dual buffer layer (Cell-55) degrades less (5.13%) as compared to that of the cells (Cell-49) with single buffer (7.72%). Due to the better nucleation zone of the i-layer on the mso-2 layer compared to mso-1 layer, i-layer becomes more compact and less degrades against light irradiation

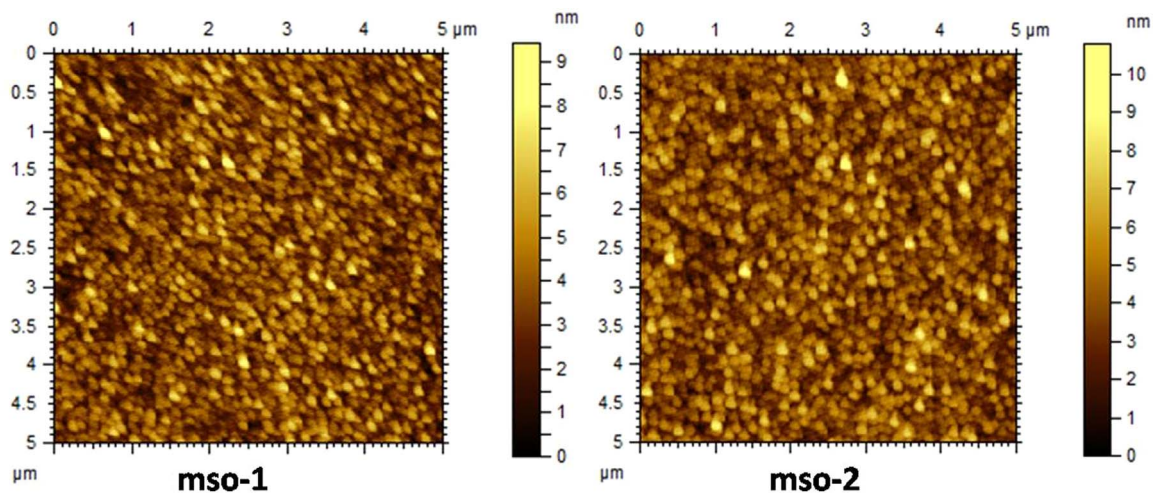



Fig. 6. AFM micrograph of the mso-1 and mso-2 films.

Glass			
ZnO:Al			
			
	p- μ c-SiO:H	200Å	
mso-1	i- μ c-SiO:H	60Å	
<div>i-μc-Si:H</div> <div>2μm</div>			
n- μ c-SiO:H			300Å
Al			3000Å
Cell 49			

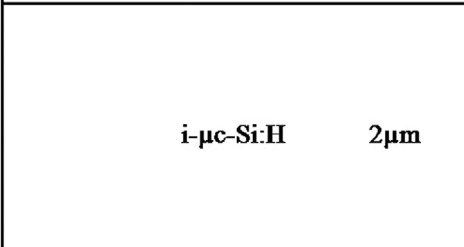
Glass			
ZnO:Al			
			
	p- μ c-SiO:H	200Å	
mso-1	i- μ c-SiO:H	30Å	
mso-2	i- μ c-SiO:H	40Å	
<div>i-μc-Si:H</div> <div>2μm</div>			
n- μ c-SiO:H			300Å
Al			3000Å
Cell 55			

Fig. 8. Cell structure without dual buffer (Cell 49), with dual buffer layer (Cell-55).

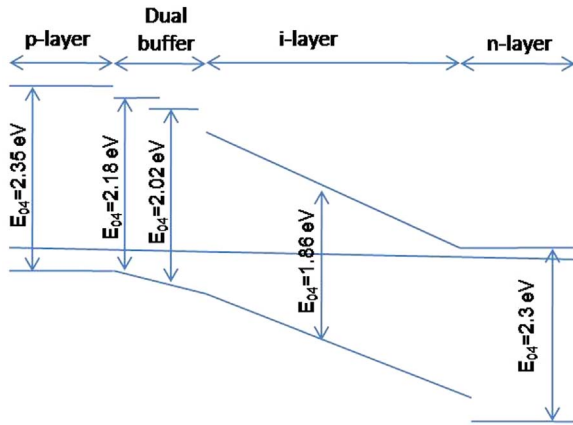


Fig. 9. Schematic energy band diagram of the single junction μ c-Si:H cell with dual buffer concept.

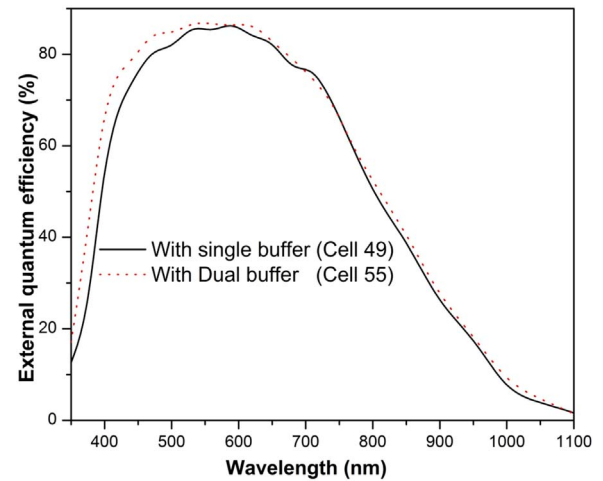


Fig. 11. EQE curve of cells without dual buffer layer and with dual buffer layer.

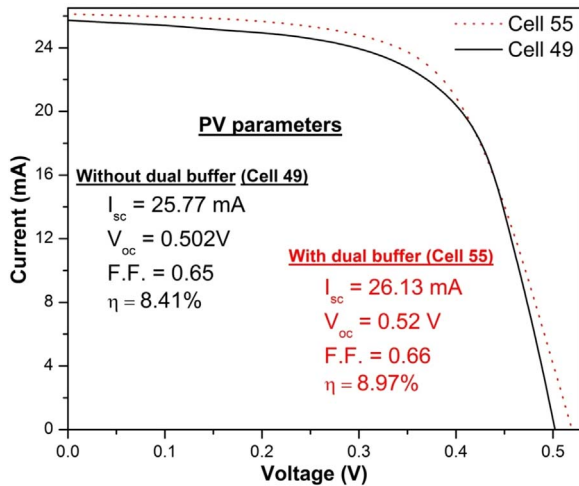


Fig. 10. I-V characteristics of cells without dual buffer layer and with dual buffer layer at the p/i interface.

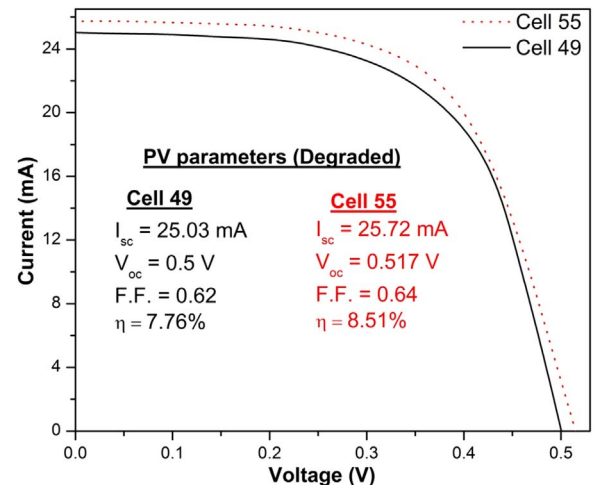


Fig. 12. I-V curves of the cells (Cell-49 and Cell-55) after 600 h of light soakings.

Degraded *I-V* characteristics of the both cells are shown in Fig. 12.

4. Conclusion

Two intrinsic $\mu\text{-SiO}_x\text{:H}$ films with two different E_{04} have been successfully developed for dual buffer layer for $\mu\text{-Si:H}$ solar cell. The effects of two thin microcrystalline $\text{SiO}_x\text{:H}$ layers as dual buffer layer, inserted at the p/i interface of a $\mu\text{-Si:H}$ thin-film solar cells have been studied. Noteworthy improvement in output PV parameters is detected for the solar cells deposited at high power pressure regime. Dual buffer layer helps to terminate the band-gap mismatching problem between high optical gap window layer and i-layer of $\mu\text{-Si:H}$ solar cells. Second buffer layer is also promoting the growth of the intrinsic active layer as X_c of second buffer layer is higher than that of first buffer layer, $\mu\text{-Si:H}$ i-layer finds the better nucleation or growth center on the top of second buffer. Further improvement is also possible after better optimization and insertion of extra buffer layer at the interface. Less degradation is also noticed in the solar cell with dual buffer layer at the p/i interface.

Acknowledgment

This work has been supported by Ministry of New and Renewable Energy (MNRE) (31/40/2010-11/PVSE), Govt. of India. Gourab Das gratefully acknowledges DST-INSPIRE Programme Division (Govt. of India) for their financial support. We thank Prof. H. Saha for his support in all aspects.

References

- [1] D.L. Staebler, C.R. Wronski, Reversible conductivity changes in discharge-produced amorphous Si, *Appl. Phys. Lett.* 31 (4) (1977) 292.
- [2] Y. Wang, X. Han, F. Zhu, G. Hou, H. Ren, K. Zhang, J. Xue, J. Sun, Y. Zhao, X. Geng, Light induced degradation of microcrystalline silicon solar cells, *J. Non-Cryst. Solids* 352 (2006) 1909–1912.
- [3] A.V. Shah, J. Meier, E. Vallat-Sauvain, N. Wyrsch, U. Kroll, C. Droz, U. Graf, Material and solar cell research in microcrystalline silicon, *Sol. Energy Mater. Sol. Cells* 78 (2003) 469–491.
- [4] F. Meillaud, E. Vallat-Sauvain, X. Niquille, M. Dubey, J. Bailat, A. Shah, C. Ballif, Light-induced degradation of thin film amorphous and microcrystalline silicon solar cells, *Photovoltaic Specialists Conference Conference Record of the Thirty-first IEEE*, 2005.
- [5] J. Bailat, E. Vallat-Sauvain, L. Feitknecht, C. Droz, A. Shah, Microstructure and open-circuit voltage of n-i-p microcrystalline silicon solar cells, *J. Appl. Phys.* 93 (9) (2003) 5727–5731.
- [6] S. Guha, J. Yang, P. Nath, M. Hack, Enhancement of open circuit voltage in high efficiency amorphous silicon alloy solar cells, *Appl. Phys. Lett.* 49 (1986) 218.
- [7] M.N.V. den Donker, S. Klein, B. Rech, F. Finger, W.M.M. Kessels, M.C.M. van de Sanden, Microcrystalline silicon solar cells with an open-circuit voltage above 600 mV, *Appl. Phys. Lett.* 90 (2007) 183504.
- [8] F. Finger, Y. Mai, S. Klein, R. Carius, High efficiency microcrystalline silicon solar cells with hot-wire CVD buffer layer, *Thin Solid Films* 516 (2008) 728–732.
- [9] R.E. Hollingsworth, P.K. Bhat, A. Madan, Microcrystalline and wide band gap p^+ window layers for a-Si p-i-n solar cells, *J. Non-Cryst. Solids* 97–98 (1987) 309–312.
- [10] Y. Huang, A. Dasgupta, A. Gordijn, F. Finger, R. Carius, Highly transparent microcrystalline silicon carbide grown with hot wire chemical vapor deposition as window layers in n-i-p microcrystalline silicon solar cells, *Appl. Phys. Lett.* 90 (20) (2007) 203502.
- [11] H. Tan, P. Babal, M. Zeman, A.H.M. Smets, Wide bandgap p-type nanocrystalline silicon oxide as window layer for high performance thin-film silicon multi-junction solar cells, *Sol. Energy Mater. Sol. Cells* 132 (2015) 597–605.
- [12] A. Lambert, F. Finger, B. Holländer, J.K. Rath, R.E.I. Schropp, Boron-doped hydrogenated microcrystalline silicon oxide ($\mu\text{-SiO}_x\text{:H}$) for application in thin-film silicon solar cells, *J. Non-Cryst. Solids* 358 (2012) 1962–1965.
- [13] H. Tan, L. Sivec, B. Yan, R. Santbergen, M. Zeman, A.H.M. Smets, Improved light trapping in microcrystalline silicon solar cells by plasmonic back reflector with broad angular scattering and low parasitic absorption, *Appl. Phys. Lett.* 102 (2013) 153902.
- [14] H. Sai, T. Koida, T. Matsui, I. Yoshida, K. Saito, M. Kondo, Microcrystalline silicon solar cells with 10.5% efficiency realized by improved photon absorption via periodic textures and highly transparent conductive oxide, *Appl. Phys. Express* 6 (2013) 104101.
- [15] H. Sai, T. Matsui, K. Matsubara, M. Kondo, I. Yoshida, 11.0%-efficient thin-film microcrystalline silicon solar cells with honeycomb textured substrates, *IEEE J. Photovolt.* 4 (6) (2014) 1349–1354.
- [16] G. Das, S. Mandal, S. Dhar, S. Bose, S. Mukhopadhyay, C. Banerjee, A.K. Barua, Development of n-type microcrystalline $\text{SiO}_x\text{:H}$ films and its application by innovative way to improve the performance of single junction $\mu\text{-Si:H}$ solar cell, *J. Mater. Sci.: Mater. Electron.* 28 (8) (2017) 5746–5753.
- [17] M.D. Zoysa, K. Ishizaki, Y. Tanaka, H. Sai, K. Matsubara, S. Noda, Enhanced efficiency of ultrathin (> 500 nm)-film microcrystalline silicon photonic crystal solar cells, *Appl. Phys. Express* 10 (2017) 012302.
- [18] G. Das, S. Mandal, S. Dhar, S. Bose, J.R. Sharma, S. Mukhopadhyay, C. Banerjee, A.K. Barua, Development of improved n- $\mu\text{-SiO}_x\text{:H}$ films and its innovative application in silicon-based single junction thin film solar cells (PP), *IEEE J. Photovolt.* (99) (2017) 1–8, <http://dx.doi.org/10.1109/JPHOTOV.2017.2655721>.
- [19] G. Das, S. Mandal, R. Tomy M, C. Banerjee, S. Mukhopadhyay, A.K. Barua, Development of oxide based window and buffer layer for single junction amorphous solar cell: reduction of light induced degradation, *Mater. Sci. Semicond. Process.* 24 (2014) 50–56.
- [20] G. Bugnon, G. Parascandolo, S. Hänni, M. Stuckelberger, M. Charrière, M. Despeisse, F. Meillaud, C. Ballif, Silicon oxide buffer layer at the p-i interface in amorphous and microcrystalline silicon solar cells, *Sol. Energy Mater. Sol. Cells* 120 (2014) 143–150.
- [21] G. Lucovsky, J. Yang, S.S. Chao, J.E. Tyler, W. Czubytyj, Oxygen-bonding environments in glow-discharge-deposited amorphous silicon-hydrogen alloy films, *Phys. Rev. B* 28 (1983) 3225.
- [22] S. Ray, S. Mukhopadhyay, T. Jana, Studies on microstructure of silicon thin films and its effect on solar cells, *Sol. Energy Mater. Sol. Cells* 90 (2006) 631–639.
- [23] E. Bhattacharya, A.H. Mahan, Microstructure and the light induced meta-stability in hydrogenated amorphous silicon, *Appl. Phys. Lett.* 52 (1988) 1587–1589.
- [24] U. Kroll, J. Meier, P. Torres, J. Pohl, A. Shah, From amorphous to microcrystalline silicon films prepared by hydrogen dilution using the VHF (70 MHz) GD technique, *J. Non-Cryst. Solids* 227–230 (1998) 68–72.
- [25] A. Sarker, C. Banerjee, A.K. Barua, Preparation and characterization of n-type microcrystalline hydrogenated silicon oxide films, *J. Phys. D: Appl. Phys.* 35 (2002) 1205–1209.
- [26] S.C. Moss, J.F. Graczyk, Evidence of voids within the As deposited structure of glassy silicon, *Phys. Rev. Lett.* 23 (1969) 1167–1171.
- [27] L. Alexander, H.P. Klug, Determination of Crystallite Size with the X-Ray Spectrometer, *J. Appl. Phys.* 21 (1950) 137.